Title

Self-consistent Simulation of Supersonic Plasma Flows in Advanced Divertors

Author names and affiliations

author names (given name first)

Satoshi Togo[1], Tomonori Takizuka[2], Dirk Reiser[3], Mizuki Sakamoto[1], Naomichi Ezumi[1], Yuichi Ogawa[4], Kunpei Nojiri[1], Kenzo Ibano[2], Yue Li[4], Yousuke Nakashima[1]

affiliations

[1]Plasma Research Center, University of Tsukuba, 1-1-1 Tennodai, Tsukuba 305-8577, Japan
[2]Graduate School of Engineering, Osaka University, 1-1 Yamadaoka, Suita 565-0871, Japan
[3]Forschungszentrum Jülich GmbH, IEK-Plasmaphysik, Jülich 52425, Germany
[4]Graduate School of Frontier Sciences, University of Tokyo, 5-1-5 Kashiwanoha, Kashiwa 277-8568, Japan

Corresponding author

Satoshi Togo[1*1] (togo@prc.tsukuba.ac.jp[*2])
([*1]current affilication: ITER Organization, Route de Vinon sur Verdon, 13067 St Paul Lez Durance Cedex, France)
([*2]current e-mail address: Satoshi.Togo@iter.org)

Abstract

Advanced divertors gain larger plasma wetted area by poloidal or total flux expansion. Qualitative characteristics of supersonic plasma flows which are generated by the magnetic nozzle effect are studied by using a plasma fluid model incorporating anisotropic ion pressure (AIP model). The AIP model can self-consistently simulate supersonic plasma flows because, unlike the widely-used plasma fluid model (the Braginslii equations), the equation of parallel plasma momentum in it is described as a hyperbolic-type and the plasma flow velocity is solved without using explicit boundary conditions at the sheath entrance in front of divertor plates. In comparisons of plasma profiles between the AIP model and the Braginskii equations, it is observed that the plasma flow velocity in the Braginskii equations is forced to the sound speed at the sheath entrance in conditions of decelerating supersonic plasma flows leading to qualitative deviations with the AIP model. In an application of the AIP model to a scrape-off layer/divertor region incorporating super-X divertors with various flux-expansion ratios, supersonic plasma flows in divertor regions and highly anisotropic ion temperatures

are successfully simulated. It is also demonstrated that it becomes easier with the AIP model to explain the mechanisms of generations of supersonic plasma flows and acceleration/deceleration of them (including stationary shock waves) in flux-expanding divertors from the mirror effect point of view.

Keywords

scrape-off layer, advanced divertor, plasma fluid model, anisotropic ion pressure, Bohm criterion, supersonic plasma flows, stationary shock waves

Body of paper

1 Introduction

Development of a robust control method of the divertor heat load is one of the most important issues to commercialize tokamak fusion reactors. Divertor plasma detachment is expected to be a promising way to resolve this issue but it is pointed out that, even for ITER, the operating window for partially detached plasmas is narrow with respect to the divertor neutral pressure and the radiation fraction in the scrape-off layer (SOL)/divertor region [1, 2]. As for DEMO reactors, the operating window is thought to be much narrower or disappear with a standard divertor geometry like ITER because of the following reasons; (i) a divertor-heat-load metric P/R (P is the heating power and R is the major radius, respectively) can be 4-5 times as large as that of ITER, (ii) the maximum tolerable heat load of the divertor plate can be a half of that of ITER due to the high neutron load and (iii) the heat flux width λ_q might be smaller according to the Eich scaling [3]. For example, it is reported that the peak divertor heat load is evaluated to be 16 MW/m^2 with 92% radiation of the exhaust power in an ITER-size DEMO reactor with 3 GW fusion power [4]. Advanced divertors [5], such as snowflake divertor [6], super-X divertor (SXD) [7, 8] and X-point target divertor [9], have been expected to produce acceptable solutions to this matter. They help increase the plasma-wetted area $A_{\rm wet}$ by poloidal/total flux expansion or increasing the number of divertors (or a combination of these).

It is reported that high-Mach (including supersonic) plasma flows might occur in SOL/divertor regions of tokamak fusion plasmas in divertor-detachment states [10]. Generation of supersonic plasma flows affects the evaluation of operating windows of future fusion reactors by changing conditions of atomic and molecular (A&M) processes and impurity confinement because widely-used theoretical and numerical models assumes the Mach number of unity at the sheath entrance in front of divertor plates (i.e. the lower limit of the Bohm criterion) as briefly explained in the next paragraph. Also, it has been theoretically pointed out that in a one-dimensional (1D) compressible plasma flow a supersonic transition can be brought about by variations in the cross-sectional area (so-called a Laval nozzle), which corresponds to flux expansion and compression, as well as heat transfer and particle/momentum sources [11, 12, 13]. Experiments with a linear device HITOP actually demonstrated that supersonic plasma flows could be generated by the magnetic nozzle effect [14, 15]. Therefore, it is essen-

tial especially in evaluating the performance of advanced divertors to develop a theoretical or numerical model which self-consistently predicts a generation of a supersonic plasma flow and to conduct benchmark studies by comparing with existing experimental results.

In various kinds of advanced divertors, SXD brings about the total flux expansion and significantly increases $A_{\rm wet}$ by setting the outer divertor plate at a further position in the major radius than a standard divertor, and thus is thought to have higher possibility to generate supersonic plasma flows. Experimental data on the performance of SXD have been obtained with some tokamaks such as TCV [8] and DIII-D [16], and will be obtained with MAST Upgrade, too [17]. Some linear devices also contribute to research the performance of SXD making the most use of their flexibility on experimental conditions and diagnostics [18, 19]. In order to theoretically analyze the results from these experiments, the two-point model (TPM) modified for inhomogeneous magnetic field systems is often utilized. Although many physical processes are neglected in the TPM, it is useful for simply obtaining the downstream density $n_{\rm t}$, temperature $T_{\rm t}$ and the upstream temperature $T_{\rm u}$ as functions of the upstream density $n_{\rm u}$ [20, 16]. The TPM, however, is based on a pressure balance equation ($2n_{\rm t}T_{\rm t} = n_{\rm u}T_{\rm u}$) in which the sonic transition is assumed to be fixed at the sheath entrance. Thus, it is difficult to self-consistently treat generations of supersonic plasma flows by the TPM. As for the numerical simulation researches, some code packages such as SOLPS [21], SONIC [22, 23] and UEDGE [24] have been developed for self-consistent simulations of plasma, neutral and impurity fluids or particles in SOL/divertor regions, and have been applied to SXD, too [25, 26, 27, 28]. In these code packages, a plasma is described by a fluid model known as the Braginkii equations [29]. In the Braginskii equations, however, the effect of the parallel ion viscosity, which arises from the anisotropy of ion temperature (or pressure), is approximated in terms of the parallel gradients of the magnetic field strength and the plasma flow velocity by assuming high collisionality. Due to this, the equation of parallel plasma momentum becomes parabolic type and requires an explicit boundary condition for the plasma flow velocity at the sheath entrance (for example, the Mach number of unity). Various patterns of profiles of the plasma flow velocity can be obtained depending on the choice of this boundary condition as is demonstrated for example in Ref. [30] with SONIC. In the B2 code [31], which is the earliest one out of the various versions of the plasma fluid code used in SOLPS, an option for the boundary condition of the plasma flow velocity is prepared in which the plasma flow velocity is linearly extrapolated if it tends to be higher than the sound speed. This option, however, might lead to a non-smooth profile of plasma flow velocity [32]. Therefore, supersonic plasma flows cannot be self-consistently simulated with the Braginskii equations.

In plasma fluid models used in Refs. [33, 34, 35, 36], the equation of parallel plasma momentum is described as a hyperbolic type by neglecting the effect of parallel ion viscosity and it becomes possible to automatically determine the position of the sonic transition and the plasma flow velocity at the sheath entrance. However, it is reported from kinetic simulation results with PARASOL, a Particle-in-Cell (PIC) model combined with a Monte-Carlo binary collision model [37], that anisotropy of ion temperature remains even for marginal-collisionality plasmas [38, 39]. These plasma fluid models are, thus, limited to high-collisionality plasmas. Meanwhile, some physically interesting phenomena concerning supersonic plasma flows like stationary shock waves are observed in comparably low-collisionality plasmas [36].

We have been developing a plasma fluid model incorporating the anisotropic ion temperature [40, 41, 42, 43, 44] or pressure (AIP model) [32, 45] based on generalized plasma fluid models discussed for example in Refs. [46, 47]. By directly expressing the parallel ion viscosity in terms of the anisotropic ion temperature (or pressure) without any approximations, the equation of parallel plasma momentum is described as a hyperbolic type keeping the finite effect of the parallel ion viscosity. Therefore, our model can be used for simulating supersonic plasma flows in low-to-middle-collisionality plasmas as well as high-collisionality ones although some flux-limiting procedures are necessary for parallel conductive heat fluxes in low-to-middle-collisionality plasmas [48, 39]. Instead of using explicit boundary conditions at the sheath entrance, a virtual divertor (VD) model [41] is used which is similar to the penalization scheme [35, 13]. Our model has been reproducing the ion temperature anisotropy for various collisionality and supersonic plasma flows generated in radiative-cooling divertors evaluated by PARASOL [40, 41]. We also have been observing supersonic plasma flows caused by the magnetic nozzle effect [43, 32, 44, 45]. Especially in Ref. [45], basic characteristics of accelerating supersonic plasma flows are investigated for high-collisionality plasmas with an SXD-like pure-poloidal magnetic field system.

The AIP model, however, still has following shortcomings compared to the plasma fluid codes included in the code packages; (i) it focuses only on the 1D parallel transport and multi-dimensional effects are included in source terms (e.g. those from core plasmas) or neglected, (ii) it does not consider impurity effects and uses a simple quasi-neutrality condition (i.e. ion and electron densities are the same) and (iii) it is not coupled with any sophisticated neutral codes (e.g. EIRENE [49] and NEUT2D [50]) and impurity codes (e.g. IMPGYRO [51] and IMPMC [52]). It is, hence, still not adequate to quantitatively study the performance of kinds of divertors by using the AIP model at the present stage. In this paper, therefore, we further study qualitative characteristics of supersonic plasma flows generated due to the magnetic nozzle effect including decelerating supersonic plasma flows and low-collisionality cases. We first compare solutions from the AIP model with those from the B2 code which is based on the Braginskii equations in cases of decelerating supersonic plasma flows by using pure-poloidal magnetic field systems in order to obtain qualitative insights more simply. After that, we apply the AIP model to an SOL/divertor system of ~ 20 m parallel length with SXDs and investigate characteristics of supersonic plasma flows focusing on effects of the flux expansion ratio and ionization source in front of divertor plates.

In the following section, the AIP model, the B2 code and a simple neutral model used with the AIP model are briefly explained. In Sec. 3, results of comparison between the AIP model and the B2 code are shown. Results of the application of the AIP model to an SOL/divertor system with SXDs are presented in Sec. 4. Finally, we draw a conclusion in Sec. 5.

2 Numerical models

2.1 Anisotropic-ion-pressure (AIP) model

The basic equations in the AIP model [32] are summarized as follows;

$$\frac{\partial n}{\partial t} + B\frac{\partial}{\partial s}\left(\frac{nV}{B}\right) = S, \tag{1}$$

$$\frac{\partial}{\partial t}\left(m_{\rm i} nV\right) + B\frac{\partial}{\partial s}\left[\frac{1}{B}\left(m_{\rm i} nV^2 + p_{\rm i,\parallel} + p_{\rm e}\right)\right] + \frac{p_{\rm i,\perp} + p_{\rm e}}{B}\frac{\partial B}{\partial s} = M_{\rm m}, \tag{2}$$

$$\begin{aligned}&\frac{\partial}{\partial t}\left(\frac{1}{2}m_{\rm i} nV^2 + \frac{1}{2}p_{\rm i,\parallel}\right) + B\frac{\partial}{\partial s}\left[\frac{1}{B}\left(\frac{1}{2}m_{\rm i} nV^3 + \frac{3}{2}p_{\rm i,\parallel}V + q_{\rm i,\parallel}\right)\right] + \frac{p_{\rm i,\perp}V + q_{\rm i,\perp}}{B}\frac{\partial B}{\partial s}\\ &= Q_{\rm i,\parallel} + \frac{p_{\rm i,\perp} - p_{\rm i,\parallel}}{\tau_{\rm rlx}} + \frac{m_{\rm e}}{m_{\rm i}}\frac{p_{\rm e} - p_{\rm i,\parallel}}{\tau_{\rm e}} - V\frac{\partial p_{\rm e}}{\partial s},\end{aligned} \tag{3}$$

$$\frac{\partial p_{\rm i,\perp}}{\partial t} + B\frac{\partial}{\partial s}\left(\frac{p_{\rm i,\perp}V + q_{\rm i,\perp}}{B}\right) - \frac{p_{\rm i,\perp}V + q_{\rm i,\perp}}{B}\frac{\partial B}{\partial s} = Q_{\rm i,\perp} + \frac{p_{\rm i,\parallel} - p_{\rm i,\perp}}{\tau_{\rm rlx}} + \frac{2m_{\rm e}}{m_{\rm i}}\frac{p_{\rm e} - p_{\rm i,\perp}}{\tau_{\rm e}}, \tag{4}$$

$$\frac{\partial}{\partial t}\left(\frac{3}{2}p_{\rm e}\right) + B\frac{\partial}{\partial s}\left[\frac{1}{B}\left(\frac{5}{2}p_{\rm e}V + q_{\rm e}\right)\right] = Q_{\rm e} + \frac{3m_{\rm e}}{m_{\rm i}}\frac{p_{\rm i} - p_{\rm e}}{\tau_{\rm e}} + V\frac{\partial p_{\rm e}}{\partial s}. \tag{5}$$

Equations (1)-(5) describe the parallel transport of ion particles, parallel plasma momentum, parallel ion energy, perpendicular ion energy and (isotropic) electron energy, respectively. The notations included in these equations are the same as those in Ref. [32]. The ion-pressure relaxation time $\tau_{\rm rlx} = 2.5\tau_{\rm i}$ [46] is estimated by using the effective-isotropic ion temperature $T_{\rm i} \equiv \left(T_{\rm i,\parallel} + 2T_{\rm i,\perp}\right)/3$. The validity of this model is numerically confirmed by a kinetic simulation with a binary collision model [37]. These equations are simultaneously solved with the equation of state $p_\sigma = nT_\sigma$ in which σ stands for the species and components as $\sigma \in \{({\rm i},\parallel),\ ({\rm i},\perp),\ {\rm i},\ {\rm e}\}$. Note that Eq. (2) is hyperbolic and, thus, does not require an explicit boundary condition on V. Note also that Eq. (2) is written in the conservative form and that it is equivalent to those in earlier works such as Refs. [53, 54].

The parallel conductive heat fluxes of parallel and perpendicular components of ion energy, $q_{\rm i,\parallel}$ and $q_{\rm i,\perp}$ in Eqs. (3) and (4), are given by a flux-limiting procedure like $q_{\rm i,\parallel} = \left[1/q_{\rm i,\parallel}^{\rm SH} + 1/\left(\alpha_{\rm i,\parallel}q_{\rm i,\parallel}^{\rm FS}\right)\right]^{-1}$ and $q_{\rm i,\perp} = \left[1/q_{\rm i,\perp}^{\rm SH} + 1/\left(\alpha_{\rm i,\perp}q_{\rm i,\perp}^{\rm FS}\right)\right]^{-1}$. Here, $q_{\rm i,\parallel}^{\rm SH}$ and $q_{\rm i,\perp}^{\rm SH}$ are evaluated by using the Spitzer-Härm (SH) parallel ion heat conductivity $\kappa_{\rm i}^{\rm SH} = 3.9n\tau_{\rm i}T_{\rm i,\parallel}/m_{\rm i}$ [55, 29] like $q_{\rm i,\parallel}^{\rm SH} = -\left(1/3\right)\kappa_{\rm i}^{\rm SH}\left(\partial T_{\rm i,\parallel}/\partial s\right)$ and $q_{\rm i,\perp}^{\rm SH} = -\left(2/3\right)\kappa_{\rm i}^{\rm SH}\left(\partial T_{\rm i,\perp}/\partial s\right)$, in which 1/3 and 2/3 correspond to the degree of freedom in the parallel and perpendicular directions. The free-streaming (FS) heat fluxes are given by $q_{\rm i,\parallel}^{\rm FS} = \left(1/3\right)nT_{\rm i,\parallel}\sqrt{T_{\rm i,\parallel}/m_{\rm i}}$ and $q_{\rm i,\perp}^{\rm FS} = \left(2/3\right)nT_{\rm i,\perp}\sqrt{T_{\rm i,\parallel}/m_{\rm i}}$. The ion heat-flux-limiting factors, $\alpha_{\rm i,\parallel}$ and $\alpha_{\rm i,\perp}$, are set to be infinity in Sec. 3 because the ion heat-flux-limiting factor is not available in the B2 code while $\alpha_{\rm i,\parallel} = \alpha_{\rm i,\perp} = 0.5$ are used in Sec. 4. The parallel conductive heat flux of electron, $q_{\rm e}$ in Eq. (5), is also given by $q_{\rm e} = \left[1/q_{\rm e}^{\rm SH} + 1/\left(\alpha_{\rm e}q_{\rm e}^{\rm FS}\right)\right]^{-1}$ with $q_{\rm e}^{\rm SH} = -\kappa_{\rm e}^{\rm SH}\left(\partial T_{\rm e}/\partial s\right)$ (the SH parallel electron heat conductivity $\kappa_{\rm e}^{\rm SH} = 3.16n\tau_{\rm e}T_{\rm e}/m_{\rm e}$ [55, 29]) and $q_{\rm e}^{\rm FS} = nT_{\rm e}\sqrt{T_{\rm e}/m_{\rm e}}$. The electron heat-flux-limiting factor is set to be $\alpha_{\rm e} = 0.2$.

Note that the present models of the parallel conductive heat fluxes are tentative ones. Parallel gradients of the temperature occurs spontaneously in inhomogeneous magnetic fields due to magnetic moment conservation [44]. It is, hence, no longer adequate in inhomogeneous magnetic fields to describe the parallel conductive heat fluxes such that they are simply proportional to parallel gradients of the temperature like those used in this paper. Developing appropriate models of the parallel conductive heat fluxes in inhomogeneous magnetic fields is one of our future works. In Sec. 3, we choose comparably high-collisionality plasmas so that the fraction of the parallel conductive heat fluxes of ion to convective ones becomes small enough. It becomes small enough in Sec. 4, too, thanks to the flux-limiting procedure. Therefore, the models of the parallel conductive heat fluxes of ion do not have a controlling impact on the presented results.

2.2 B2 code (Braginskii equation)

For a comparison between the AIP model and the Braginskii equations, we also use a plasma fluid code B2 [31]. In order to identify the calculation conditions with the AIP model, all of the radial transport terms are turned off. Then, the equation of parallel plasma momentum solved in the B2 code is obtained by describing Eq. (2) in terms of the isotropic and anisotropic parts of the ion pressure, $p_\mathrm{i} \equiv \left(p_{\mathrm{i},\parallel} + 2p_{\mathrm{i},\perp}\right)/3$ and $\delta p_\mathrm{i} \equiv 2\left(p_{\mathrm{i},\parallel} - p_{\mathrm{i},\perp}\right)/3$ instead of $p_{\mathrm{i},\parallel}$ and $p_{\mathrm{i},\perp}$ as follows;

$$\frac{\partial}{\partial t}\left(m_\mathrm{i} n V\right) + B\frac{\partial}{\partial s}\left(\frac{m_\mathrm{i} n V^2}{B}\right) + B^{3/2}\frac{\partial}{\partial s}\left(B^{-3/2}\delta p_\mathrm{i}\right) = -\frac{\partial}{\partial s}\left(p_\mathrm{i} + p_\mathrm{e}\right) + M_\mathrm{m}. \tag{6}$$

Also, the equation of (isotropic) ion energy solved in the B2 code is obtained by summing Eqs. (3) and (4) as follows;

$$\begin{aligned}&\frac{\partial}{\partial t}\left(\frac{1}{2}m_\mathrm{i} n V^2 + \frac{3}{2}p_\mathrm{i}\right) + B\frac{\partial}{\partial s}\left[\frac{1}{B}\left(\frac{1}{2}m_\mathrm{i} n V^3 + \frac{5}{2}p_\mathrm{i} V + \delta p_\mathrm{i} V + q_\mathrm{i}^\mathrm{SH}\right)\right]\\ &= Q_\mathrm{i} + \frac{3m_\mathrm{e}}{m_\mathrm{i}}\frac{p_\mathrm{e} - p_\mathrm{i}}{\tau_\mathrm{e}} - V\frac{\partial p_\mathrm{e}}{\partial s}.\end{aligned} \tag{7}$$

Here, we define $q_\mathrm{i}^\mathrm{SH} \equiv q_{\mathrm{i},\parallel}^\mathrm{SH} + q_{\mathrm{i},\perp}^\mathrm{SH}$ and $Q_\mathrm{i} \equiv Q_{\mathrm{i},\parallel} + Q_{\mathrm{i},\perp}$. It is possible to obtain an equation of δp_i from Eqs. (3) and (4) but instead of solving such an equation, δp_i is given by an approximation derived under an assumption of high collisionality (i.e. $\delta p_\mathrm{i} \ll p_\mathrm{i}$) as follows;

$$\delta p_\mathrm{i} \approx -\eta_\mathrm{i} B^{-1/2}\frac{\partial}{\partial s}\left(B^{1/2}V\right) \equiv \pi_\mathrm{i}, \tag{8}$$

in which the parallel ion viscosity η_i is given by

$$\left(1 + \Omega_\eta\right)\eta_\mathrm{i} = \eta_\mathrm{cl} \equiv 0.96 p_\mathrm{i}\tau_\mathrm{i}, \tag{9}$$

$$\Omega_\eta = \frac{\eta_\mathrm{cl}}{\beta p_\mathrm{i}}\left|\frac{\partial V}{\partial s}\right|. \tag{10}$$

The viscous-flux-limiting factor is set to be $\beta = 4/7$ [47] in this paper. As a result, the B2 code solves Eqs. (1) and (5)-(7). Note that due to the approximation of δp_i, Eq. (6) becomes

parabolic and hence requires an explicit boundary condition on V. In this paper, we choose $V \geq c_{\rm s}$ option (the sound speed is defined by $c_{\rm s} \equiv \sqrt{(T_{\rm i} + T_{\rm e})/m_{\rm i}}$ in the B2 code) at the sheath entrance in which V is linearly extrapolated if it tends to be higher than $c_{\rm s}$ as is briefly mentioned in Sec. 1.

The minimal neutral model [56] which is incorporated in the B2 code is also used to simply study effects of ionization source on supersonic plasma flows. In this model, the only reason for the neutral flux decay is ionization reactions.

2.3 Simple neutral model

A simple neutral model which is similar to the minimal neutral model in the B2 code [56] is used with the AIP model in order to simply investigate effects of ionization sources on supersonic plasma flows in Sec. 4. In this model, neutral atoms are assumed to flow along the poloidal direction $x = s\sin\theta$. Also, we assume that the pitch angle of the magnetic field θ is fixed to be $\pi/6$ rad for simplicity. The neutral particle flux at the target plate is given by $n_{\rm n}V_{\rm n} = -\rho n V \sin\theta$ in which the notations $n_{\rm n}$, $V_{\rm n}$ and ρ represent the neutral density, the neutral flow velocity and the recycling ratio at the target plate, respectively. The neutral flow $V_{\rm n}$ is given by $(V/|V|)\,V_{\rm n} = -\sqrt{2\epsilon_{\rm i}/m_{\rm i}}$ with $\epsilon_{\rm i} = 5$ eV. As for atomic processes, only is the ionization reaction considered based on the same reaction rate $\langle\sigma v\rangle_{\rm iz}$ with the minimal neutral model and the ionization source is evaluated by $S_{\rm iz} = n n_{\rm n}\langle\sigma v\rangle_{\rm iz}$. The energy source due to ionization reactions $Q_{\rm i,iz,\parallel} = (1/3)\,\epsilon_{\rm i}S_{\rm iz}$, $Q_{\rm i,iz,\perp} = (2/3)\,\epsilon_{\rm i}S_{\rm iz}$ and $Q_{\rm e,iz} = \epsilon_{\rm e}S_{\rm iz}$ with $\epsilon_{\rm e} = -25$ eV are given to Eqs. (3)-(5), respectively.

3 Comparison of Profiles between Two Plasma Fluid Models

3.1 Driving potentials of acceleration/deceleration of the plasma flow

First, we compare profiles obtained from the AIP model and the B2 code focusing on cases of decelerating supersonic plasma flows. Note here that profiles obtained from these two models quantitatively agree except for a narrow region in front of the sheath and that those in this narrow region also agree at least qualitatively when the plasma is high collisional and the plasma flow in front of the sheath is accelerating [32]. In order to consider conditions of acceleration/deceleration of plasma flows, it is convenient to derive the equation of the parallel gradient of V or the Mach number $M \equiv V/c_{\rm s}$ by combining Eqs. (1) and (2) in the steady state as follows;

$$\left(c_{\rm s}^2 - V^2\right)\frac{{\rm d}V}{{\rm d}s} = \left(c_{\rm s}^2 + V^2\right)\frac{S}{n} + 2Vc_{\rm s}\frac{{\rm d}c_{\rm s}}{{\rm d}s} + \tilde{c}_{\rm s}^2\frac{V}{B}\frac{{\rm d}B}{{\rm d}s}, \tag{11}$$

$$\left(1 - M^2\right)\frac{{\rm d}M}{{\rm d}s} = \frac{1+M^2}{nc_{\rm s}}S + \frac{M\left(1+M^2\right)}{c_{\rm s}}\frac{{\rm d}c_{\rm s}}{{\rm d}s} + \frac{\tilde{c}_{\rm s}^2}{c_{\rm s}^2}\frac{M}{B}\frac{{\rm d}B}{{\rm d}s}. \tag{12}$$

Here, the sound speed is defined by $c_{\rm s} \equiv \sqrt{\left(T_{\rm i,\parallel} + T_{\rm e}\right)/m_{\rm i}}$ in the AIP model. Also, $\tilde{c}_{\rm s} \equiv \sqrt{\left(T_{\rm i,\perp} + T_{\rm e}\right)/m_{\rm i}}$ is introduced for convenience. The contribution of the momentum source $M_{\rm m}$ is omitted because it is set to be zero in the following study. According to Eq. (12), it is a necessary condition (not a sufficient condition) at the sonic transition point (i.e. $M = \pm 1$) that the right hand side (RHS) changes its sign from positive to negative along the plasma flow. This condition is thought to be much easier to realize with advanced divertors since the RHS of Eq. (12) will become positive in the SOL region (i.e. above the X-point) due to the particle source from the core plasma and then might be negative in the divertor region (i.e. below the X-point) due to flux expansion (i.e. $M{\rm d}B/{\rm d}s < 0$). Whether the plasma flow becomes supersonic or not is actually determined by the balance among the terms in the RHS of Eq. (12).

Let us think about conditions of decelerating supersonic plasma flows. In order for a supersonic plasma flow to decelerate, the RHS of Eq. (11) should be positive. In a basic understanding of an SOL/divertor plasma [57], $V{\rm d}c_{\rm s}/{\rm d}s < 0$ holds. Meanwhile, artificial change or control of the signs of S and $V{\rm d}B/{\rm d}s$ is comparably easy. In this section, therefore, we examine two cases of decelerating supersonic plasma flows; (i) by flux compression (i.e. $V{\rm d}B/{\rm d}s > 0$) in Sec. 3.2 and (ii) by ionization source (i.e. $S > 0$) in Sec. 3.3. Note that generated plasmas in this section are always highly collisional, which enables us to exclude the issue of the validity of the $\delta p_{\rm i}$-approximation (i.e. Eq. (8)) and focus on that of the boundary condition. Note also that we use pure-poloidal magnetic field systems in this section in order to obtain qualitative insights more simply.

3.2 Effect of flux compression

First, we examine effects of flux compression on a supersonic plasma flow by using a diverging-to-contracting magnetic field system as shown in Fig. 1 (a). Here, a mirror symmetry point (i.e. $\partial n/\partial s = V = \partial T_\sigma/\partial s = 0$) and a target plate (i.e. sheath entrance) position are set at $s = 0$ and $s = L_{\rm t}$, respectively. The minimum neutral model in the B2 code is turned off and all source terms are given by input. A Gaussian-shape volumetric particle source is given like $S = S_0 \exp\left[-20\left(s/L_{\rm t}\right)^2\right]$. No volumetric momentum source is introduced (i.e. $M_{\rm m} = 0$). Also, $Q_{\rm i} = Q_{\rm e} = (3/2)T_{\rm in}S$ with the source temperature $T_{\rm in}$ are given as volumetric heat sources. For the AIP model, $Q_{\rm i}$ is isotropically divided into $Q_{\rm i,\parallel} = Q_{\rm i}/3$ and $Q_{\rm i,\perp} = 2Q_{\rm i}/3$, respectively. Figure 1 (b)-(e) shows the result of a direct comparison of plasma profiles between the B2 code and the AIP model. Note that the physical quantities are normalized by $L_{\rm t}$, $B_0 = B\left(s = 0\right)$, $T_{\rm in}$, $c_0 = \sqrt{T_{\rm in}/m_{\rm i}}$ and $n_0 = S_0 L_{\rm t}/c_0$. In both models, the plasma flow becomes supersonic at around $s/L_{\rm t} \sim 0.25$ as shown in Fig. 1 (c) because the contribution of S becomes low enough and that of the diverging magnetic field becomes dominant in Eq. (11). In the downstream contracting magnetic field region, as shown in Fig. 1 (c'), the plasma flow in the AIP model slightly decelerates (the slight acceleration just in front of the sheath entrance is probably caused by a finite effect of the numerical viscosity [41]) but keeps supersonic ($M \sim 2.5$ in the AIP model). The plasma flow in the B2 code, on the other hand, is forced to be $c_{\rm s}$ (i.e. $M = 1$) at $s = L_{\rm t}$ and rapidly decelerates at $s/L_{\rm t} \sim 0.8$. This difference is caused by the option we choose for the boundary condition on V in the B2 code by which the plasma flow is probably forced to be its lower limit (i.e.

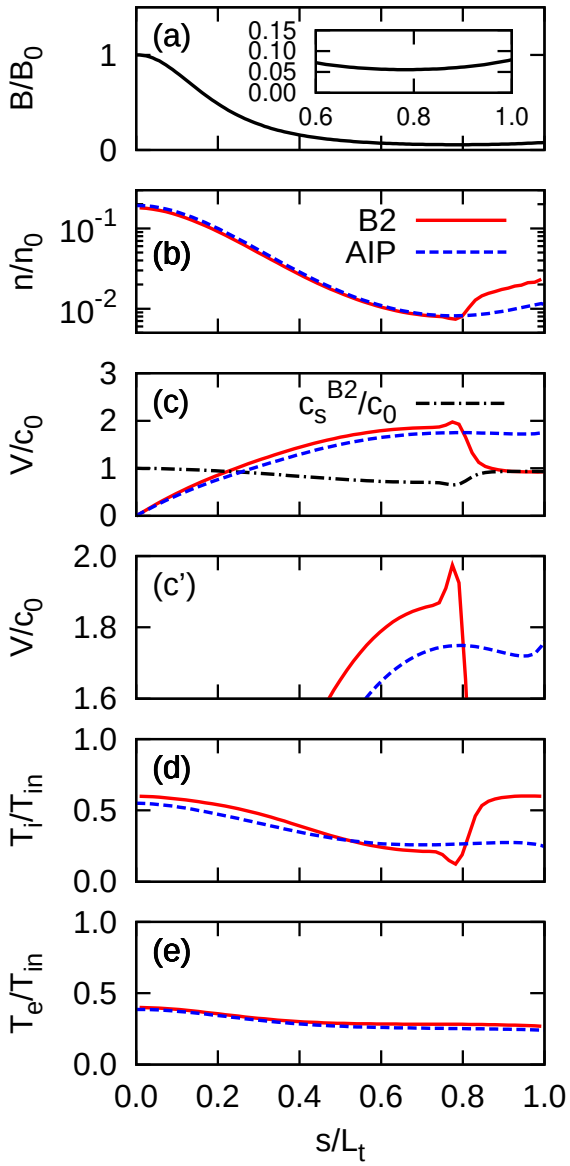

Figure 1: Comparison of parallel-to-$\boldsymbol{B}$ profiles from the B2 code (solid lines) and the AIP model (broken lines); (a) the magnetic field strength B with an enlarged view, (b) the plasma density n, (c) the plasma flow velocity V with the sound speed c_s evaluated by the B2 code (chain line) and (c') its enlarged view, (d) effective isotropic ion temperature T_i and (e) electron temperature T_e.

$V = c_\mathrm{s}$) if the plasma flow is decelerating in front of the target plate. This difference in V profiles directly affects the n profiles. In the contracting magnetic field region, n of the B2 code is about twice as large as that of the AIP model in the present calculation conditions as shown in Fig. 1 (b), which may also affect an estimation of A&M processes and conditions for plasma detachment. At the point of rapid deceleration ($s/L_\mathrm{t} \sim 0.8$), T_i rapidly increases in the B2 code as shown in Fig. 1 (d) because the flow energy turns into the internal energy. On the other hand, T_e profile is comparably flat as shown in Fig. 1 (e) because of the high parallel conductivity.

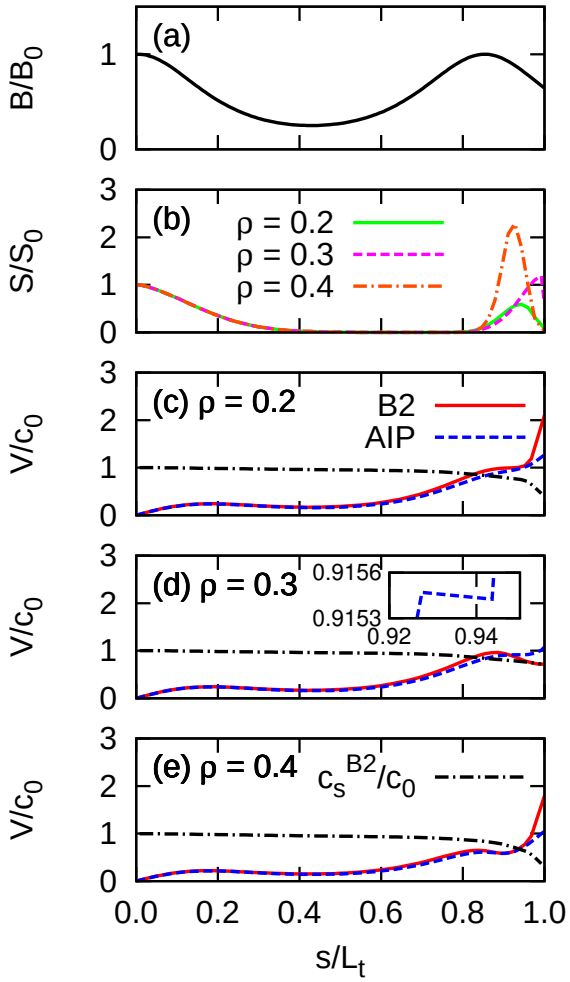

Figure 2: Parallel-to-$\boldsymbol{B}$ profiles of (a) the magnetic field strength B, (b) particle source S obtained for $\rho = 0.2$ (solid line), 0.3 (broken line) and 0.4 (chain line), and comparisons of V profiles from the B2 code (solid lines) and the AIP model (broken lines) for (c) $\rho = 0.2$, (d) 0.3 with an enlarged view and (e) 0.4 with c_s profiles evaluated by the B2 code (chain lines) for each case.

3.3 Effect of ionization source

Secondly, we examine effects of ionization source on a supersonic plasma flow by turning on the minimal neutral model in the B2 code. Here, we use a system shown in Fig. 2 (a) with the same boundary conditions with Sec. 3.2. Due to the diverging magnetic field region in front of the target plate, accelerating supersonic plasma flows are generated when there is no ionization source.

The recycling ratio ρ at the target plate is changed in a range of $0 \leq \rho \leq 0.4$. Figure 2 (b) shows S profiles obtained for $\rho = 0.2$, 0.3 and 0.4. Compared to the $\rho = 0.2$ and 0.4 cases, the peak of S shifts toward the target plate in the $\rho = 0.3$ case. These S profiles and corresponding Q_σ profiles considering the effects of energy gain/loss due to ionization reactions are shared with the AIP model. Results of comparisons of V profiles between the B2 code and the AIP model for $\rho = 0.2$, 0.3 and 0.4 are shown in Fig. 2 (c)-(e), respectively. In Fig. 3, V and c_s at the sheath entrance are shown as functions of ρ. Figure 3 shows that,

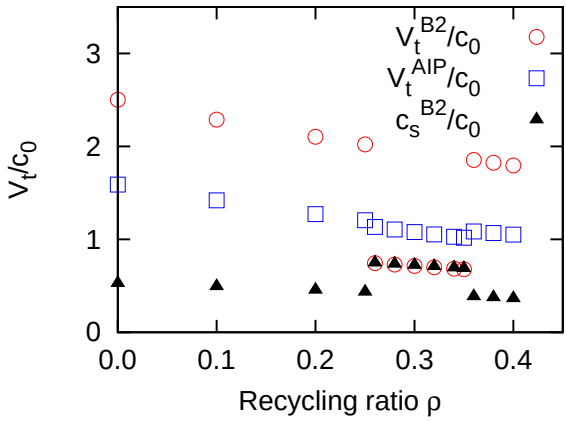

Figure 3: Plasma flow velocities at the sheath entrance V_t from the B2 code (circles) and the AIP model (squares), and the sound speed c_s at the sheath entrance from the B2 code (triangles) as functions of ρ.

at the sheath entrance, V in the B2 code is forced to be c_s in the range of $0.25 < \rho < 0.36$ in the present calculation conditions. Therefore, the cases of $\rho = 0.2$, 0.3 and 0.4 shown in Fig. 2 (c)-(e) are typical ones in three different regimes in Fig. 3. For $\rho = 0.2$, the contribution of the ionization source is small and that of the diverging magnetic field is still dominant in Eq. (11). Thus, V in the AIP model becomes sonic near the local maximum of B (i.e. $s/L_t \sim 0.85$) and continues to accelerate in the diverging magnetic field region as shown in Fig. 2 (c). In this case, V in the B2 code also has a qualitatively similar profile. For $\rho = 0.3$, the contribution of the ionization source becomes large enough to dominate that of the diverging magnetic field in Eq. (11) near the target plate. Hence, V in the AIP model becomes sonic at $s/L_t \sim 0.85$ again but slightly decelerates in the diverging magnetic field region as shown in Fig. 2 (d) (the slight acceleration just in front of the target is probably caused by a finite effect of the numerical viscosity [41]). In this condition, V at the sheath entrance is forced to be c_s in the B2 code just like the case in Sec. 3.2. This sudden decrease in V at the sheath entrance as a function of ρ is consistent with the shift of the peak of S shown in Fig. 2 (b) because n at the sheath entrance inversely shows a sudden increase which directly increases ionization reactions. For $\rho = 0.4$, the contribution of the ionization source becomes even larger to dominate that of the diverging magnetic field in Eq. (11) near the entrance of the diverging magnetic field region. Therefore, V in the AIP model can no longer become sonic at $s/L_t \sim 0.85$ but becomes sonic at $s/L_t \sim 0.94$ at which the ionization source becomes small enough and, then, accelerates toward the target plate. In this case, like the $\rho = 0.2$ case, V in the B2 code also has a qualitatively similar profile.

As a brief consequence of Sec. 3, it is indicated from Sec. 3.2 and 3.3 that the option for the boundary condition on V we choose in the B2 code in this study leads to qualitative agreements with the AIP model for accelerating supersonic plasma flows toward the target plate but to qualitative disagreements for decelerating ones. Although the situation seen in Sec. 3.2 is an extreme example compared to realistic experiments, a gradual increase in the recycling ratio in a diverging-magnetic-field system seen in Sec. 3.3 is expected in experiments of advanced divertors [8]. It is also qualitatively shown from the behavior of S profiles in Fig. 2 (b) that a self-consistent treatment of supersonic plasma flows is essential for evaluating A&M processes.

4 Application of the AIP model to an SOL/Divertor system with SXDs

4.1 Description of the system

In this section, the AIP model is applied to an SOL/Divertor system incorporating SXDs with different flux expansion ratio. We also investigate effects of ionization sources on supersonic plasma flows by using a simple neutral model explained in Sec. 2.3. A single-null configuration of a medium-size tokamak with the inverse aspect ratio ϵ of 1/4 is considered. The region from the top of the SOL ($s = 0$) to the outer divertor plate ($s = L_{\rm d} = 18$ m) is simulated. A mirror symmetry condition is assumed at $s = 0$ like Sec. 3 for simplicity. The midplane and the X-point are located at $s = L_{\rm m} = 6$ m and $s = L_{\rm X} = 12$ m, respectively. It is assumed that B at $s = 0$ and $s = L_{\rm X}$ are the same, B_0. Also, B at $s = L_{\rm m}$ is assumed to be simply given by $B_0/(1+\epsilon)$ due to the relationship of $B \sim B_0\,(R_0/R)$ (R is the major radius). At the divertor plate, $B = B_{\rm d}$ is given by $B_{\rm d} = B_0/f_{\rm exp}$ in which $f_{\rm exp}$ is the (total) flux expansion ratio. At other positions, B is given by a linear interpolation of B^{-1} from these three points. For SXDs, $f_{\rm exp}$ is set to be 1.2 and 1.5. For a comparison, $f_{\rm exp} = 0.8$ and 1 are also examined. We assume that the parallel length of the divertor region (i.e. $L_{\rm d} - L_{\rm X} = 6$ m) does not change for different $f_{\rm exp}$ for simplicity. The pitch angle of the magnetic field is fixed to be $\theta = \pi/6$ rad for simplicity as explained in Sec. 2.3 although θ becomes quite small near the X-point elongating the parallel length of the magnetic field lines in a realistic situation. But according to Eq. (12), the resulting M at the X-point is scarcely affected by this elongation as long as the effect of $\mathrm{d}B/\mathrm{d}s$ on M is focused on. Hence, this simplification does not qualitatively affect the profiles of M.

The particle and heat inputs from the core plasma are set to be $\Gamma_{\rm sep} = 2 \times 10^{22}$ /s and $P_{\rm sep} = 4$ MW, respectively, which are similar to those in medium-size tokamaks [58]. These are distributed homogeneously in the SOL region (i.e. $s = 0 \sim 12$ m) by dividing them by the volume of the SOL $K_{\rm SOL}$ like $S = \Gamma_{\rm sep}/K_{\rm SOL}$ and $Q_{\rm i,\parallel} + Q_{\rm i,\perp} + Q_{\rm e} = P_{\rm sep}/K_{\rm SOL}$. The heat sources are further divided in a similar way to Sec. 3 like $Q_{\rm i,\parallel} = (1/6)\,P_{\rm sep}/K_{\rm SOL}$, $Q_{\rm i,\perp} = (1/3)\,P_{\rm sep}/K_{\rm SOL}$ and $Q_{\rm e} = (1/2)\,P_{\rm sep}/K_{\rm SOL}$.

4.2 Effect of flux expansion

First, the plasma profiles are compared for different $f_{\rm exp}$ with $\rho = 0$ in Fig. 4. Supersonic plasma flows ($M > 1$) are obtained between the X-point and the divertor plate for $f_{\rm exp} \geq 1$ while the plasma flow is kept subsonic in almost whole region for $f_{\rm exp} = 0.8$ as shown in Fig. 4 (c). For all cases, the RHS of Eq. (11) is positive in the SOL region due to the particle input from the core plasma. In the divertor regions, on the other hand, it becomes negative for cases of $f_{\rm exp} = 1.2$ and 1.5 due to flux expansion. Even for $f_{\rm exp} = 1$ case, the RHS is negative due to the effect of the finite gradient of $c_{\rm s}$. Hence, the sonic transition occurs near the X-point in these three cases. As for $f_{\rm exp} = 0.8$ case, the RHS stays positive in the divertor region due to flux compression and, thus, the plasma flow becomes sonic at the sheath entrance. This difference in the sonic transition points affects the magnitude of n in the SOL region as shown in Fig. 4 (b).

In these sheath-limited plasmas, the difference in $f_{\rm exp}$ does not largely affect $T_{\rm e}$ as shown

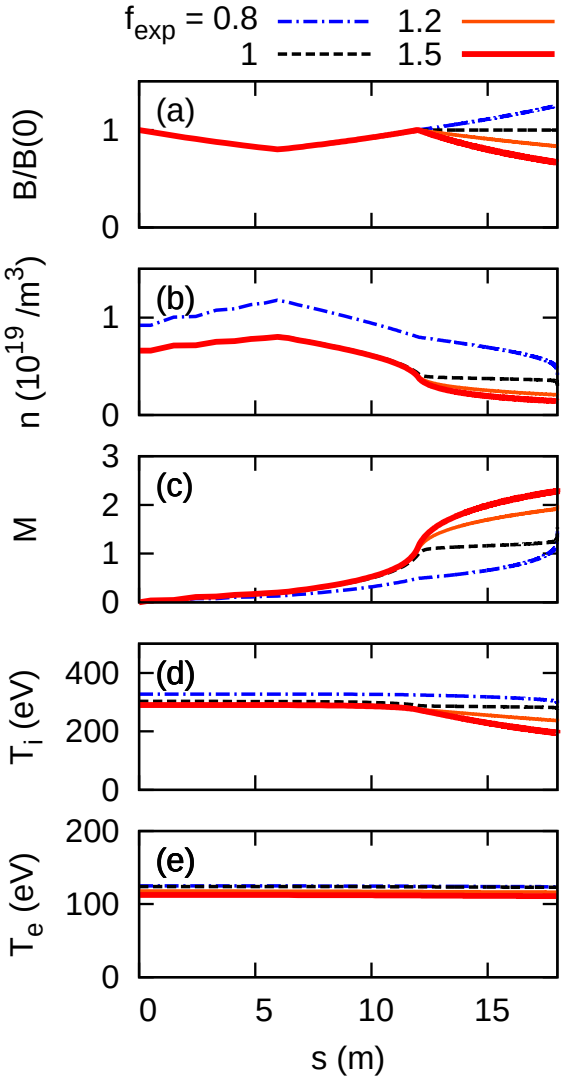

Figure 4: Parallel-to-$\boldsymbol{B}$ profiles of (a) magnetic field strength B, (b) plasma density n, (c) Mach number M, (d) effective isotropic ion temperature T_i and (e) electron temperature T_e for $f_\mathrm{exp} = 0.8$ (chain), 1 (broken), 1.2 (thin solid) and 1.5 (thick solid lines).

in Fig. 4 (e) because of the high parallel conductivity. Meanwhile, T_i profiles have negative gradients for $f_\mathrm{exp} > 1$ cases in the divertor region as shown in Fig. 4 (d). In order to see the detail, we show the profiles of $T_{\mathrm{i},\parallel}$ and $T_{\mathrm{i},\perp}$ for $f_\mathrm{exp} = 1.2$ case in Fig. 5. Note here that this T_i anisotropy comes from the difference between parallel and perpendicular components of parallel convective heat fluxes of ion [38, 40, 41] rather than the effect of inhomogeneity of the magnetic field. The negative gradient of T_i $\left(\equiv \left(T_{\mathrm{i},\parallel} + 2T_{\mathrm{i},\perp}\right)/3\right)$ comes from that of $T_{\mathrm{i},\perp}$ which is brought about by an energy loss due to the mirror effect. In the parallel component of ion energy, the energy gain due to the mirror effect is mainly used to increase the flow energy. Thus, almost flat $T_{\mathrm{i},\parallel}$ is obtained in the divertor region. Also, the negative gradient of n (or p_e) in the divertor region means the formation of the parallel ambipolar electric field through the Boltzmann relationship. Therefore, the mechanisms of the acceleration of supersonic plasma flows in flux-expanding divertors are the mirror effect and the parallel

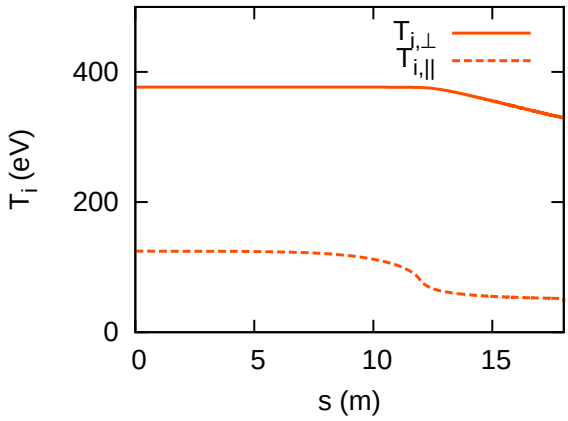

Figure 5: Parallel-to-$\boldsymbol{B}$ profiles of perpendicular $T_{\mathrm{i},\perp}$ (solid line) and parallel ion temperature $T_{\mathrm{i},\parallel}$ (broken line) for $f_{\mathrm{exp}} = 1.2$.

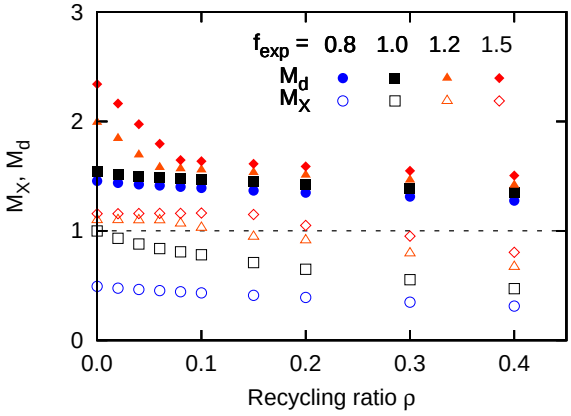

Figure 6: Mach numbers at the X-point M_{X} (open symbols) and at the sheath entrance M_{d} (closed symbols) as functions of the recycling ratio ρ; $f_{\mathrm{exp}} = 0.8$ (circles), 1 (squares), 1.2 (triangles) and 1.5 (argyles).

ambipolar electric field.

This section demonstrates the strengths of the AIP model that not only can it simulate supersonic plasma flows self-consistently, but also it can simulate plasmas with highly anisotropic ion temperature which are expected in future fusion devices. Thanks to these strengths, the acceleration of supersonic plasma flows due to the mirror effect can be explained more clearly than Braginskii-based plasma fluid models.

4.3 Effect of ionization source on plasma flows

Secondly, we change ρ in the simple neutral model in a range of $0 \leq \rho \leq 0.4$ for every f_{exp} in order to simply investigate the effect of ionization source on the plasma flow profile. Figure 6 shows the Mach numbers at $s = L_{\mathrm{X}}$ (M_{X}) and $s = L_{\mathrm{d}}$ (M_{d}) as functions of ρ. For cases of $f_{\mathrm{exp}} = 1.2$ and 1.5, M_{d} decreases comparably rapidly as ρ becomes larger until $M_{\mathrm{d}} \sim 1.5$ and $\rho \sim 0.07$ and, then, the decrement in M_{d} against ρ becomes small. This rapid decrease in M_{d} in the former phase means suppression of supersonic plasma flows near the target. The reason why $M_{\mathrm{d}} \sim 1.5$ after sufficient suppression of supersonic plasma flows is the effect

of the adiabatic index of ion $\gamma_A \approx 3$ at the sheath entrance with a more rigorous definition of the sound speed $c_s^* \equiv \sqrt{\left(\gamma_A T_{i,\parallel} + T_e\right)/m_i}$ [59]. Even in this phase, however, $M_X > 1$ cases are observed, which indicates formation of stationary shock waves like those observed in Ref. [36]. In the present calculation conditions, supersonic plasma flows are only observed in $0 \leq \rho < 0.25$ even for $f_{exp} = 1.5$ case and, thus, we investigate only in comparably low ρ region (i.e., $0 \leq \rho \leq 0.4$) in this study. However, the radial particle transport, volumetric recombination and radiation cooling, which are not considered in the present study, also help generate supersonic plasma flows. In addition, the local ρ value in the far SOL can be relatively low even though the ρ value in the whole SOL is quite high. Therefore, the practical range of ρ in which the plasma flows keep supersonic needs to be investigated by introducing the AIP model into multi-dimensional plasma fluid codes coupled with sophisticated neutral and impurity codes.

In Fig. 7, we compare the plasma profiles in $f_{exp} = 1.2$ for three typical cases; (i) $\rho = 0.02$ case in which the plasma flow becomes sonic near the X-point and is decelerated by the effect of ionization source, (ii) $\rho = 0.1$ case in which the plasma flow becomes sonic near the X-point but turns into subsonic with a stationary shock wave in the divertor region and (iii) $\rho = 0.2$ case in which the plasma flow no longer becomes sonic near the X-point and keeps subsonic. Note that these characteristics of the plasma flow for each case are confirmed in Fig. 7 (b) and that n_n at the divertor plate is proportional to $\rho/(1-\rho)$ as shown in Fig. 7 (f) due to particle conservation.

We also show the profiles of each term of the RHS of Eq. (12) for the same cases in Fig. 8. Figure 8 indicates that the magnitude of contribution of the ionization source in front of the divertor plate in the RHS of Eq. (12) and the Bohm criterion (i.e. $M_d^* \equiv V/c_s^* \geq 1$) are responsible for these three patterns of the plasma flow. From Eq. (12), the ionization source acts to decelerate supersonic plasma flows and to accelerate subsonic ones. If the ionization source is small enough, it is possible to satisfy the Bohm criterion even though the supersonic plasma flows decelerate toward the divertor plate like the $\rho = 0.02$ case. As shown in Fig. 8 (a), the RHS of Eq. (12) becomes negative in most of the divertor region due to flux expansion and the plasma flow becomes supersonic. Because it becomes positive due to the effect of ionization source in front of the target, the supersonic plasma flow decelerates but can satisfy the Bohm criterion. If the ionization source reaches a certain value which corresponds to $M_d^* = 1$, however, it is necessary for the supersonic plasma flow to turn subsonic before the ionization region because it must be slow enough to be accelerated to $M_d^* = 1$ in the ionization region. This condition leads to a formation of a stationary shock wave like the $\rho = 0.1$ case as shown in Fig. 7 (b). As shown in Fig. 8 (b), the RHS of Eq. (12) becomes negative near the divertor throat due to flux expansion and the plasma flow becomes supersonic. Then, it becomes positive due to the positive gradient of $T_{i,\parallel}$ shown in Fig. 7 (c) and decelerates the supersonic plasma flow. At the end of this positive-$T_{i,\parallel}$-gradient region, the RHS becomes negative again, at which point the plasma flow becomes subsonic forming a stationary shock wave. The RHS soon becomes positive again due to the ionization source and the plasma flow accelerates to $M_d^* = 1$. When the ionization source becomes even larger, the plasma flow no longer becomes sonic near the X-point and starts immediately to decelerate in order to be much slower at the entrance of the ionization region like the $\rho = 0.2$ case as shown in Fig. 7 (b). As shown in Fig. 8 (c), the RHS of Eq. (12) gets a slight

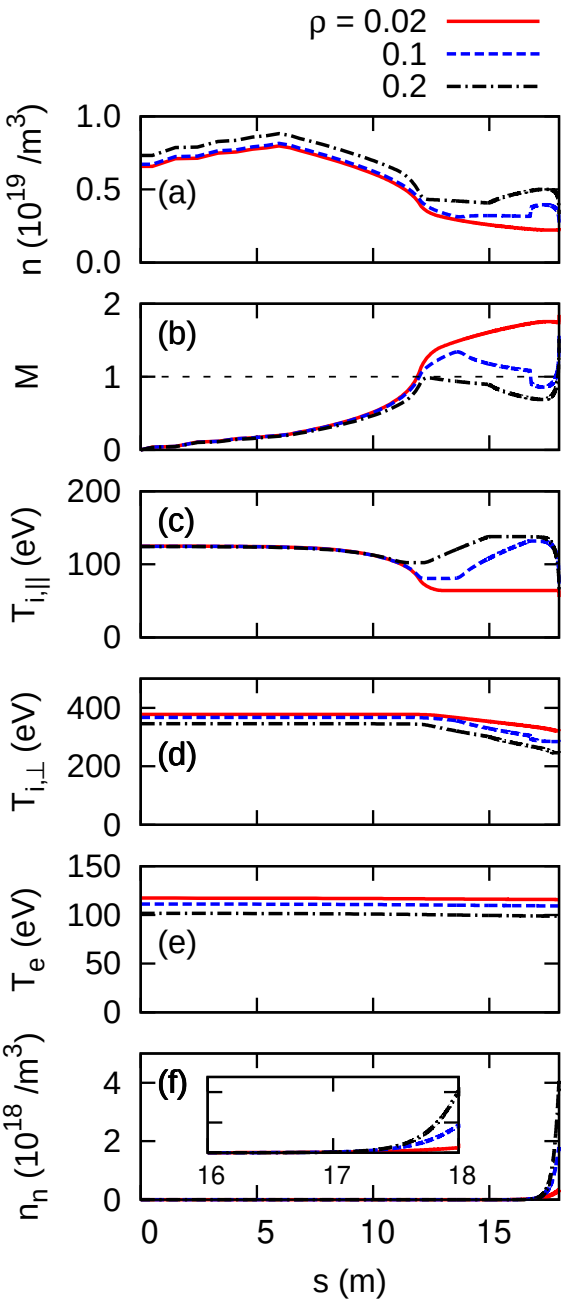

Figure 7: Parallel-to-$\boldsymbol{B}$ profiles of (a) plasma density n, (b) Mach number M, (c) parallel ion temperature $T_{\mathrm{i},\parallel}$ (d) perpendicular ion temperature $T_{\mathrm{i},\perp}$, (e) electron temperature T_{e} and (f) neutral density n_{n} with an enlarged view for $\rho = 0.02$ (solid), 0.1 (broken) and 0.2 (chain lines) in $f_{\mathrm{exp}} = 1.2$ case.

negative value because the positive gradient of $T_{\mathrm{i},\parallel}$ almost cancels the effect of flux expansion and the plasma flow keeps subsonic. Then, it becomes positive due to the ionization source in front of the divertor plate making the plasma flow accelerate to $M_{\mathrm{d}}^{*} = 1$.

As a physically interesting point of $\rho = 0.1$ case, it shows three types of different power balance between the parallel, perpendicular components of ions and electrons in the divertor region. In the region of the accelerating supersonic plasma flow (i.e. $s = 12 \sim 13.7$ m), the

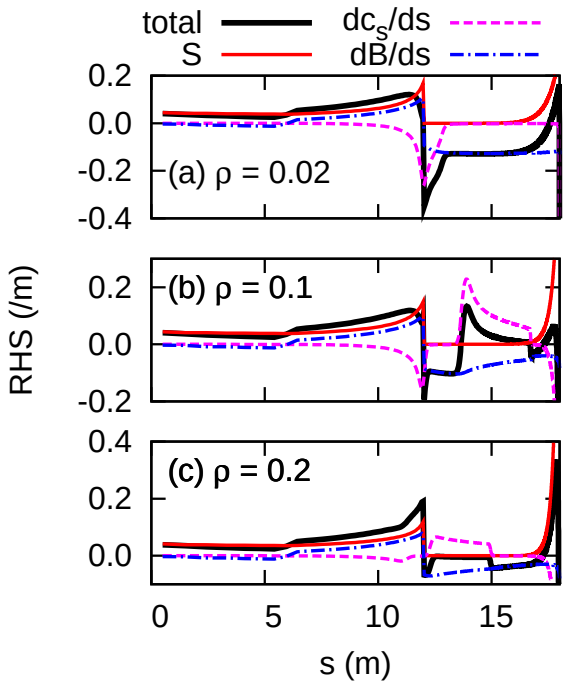

Figure 8: Parallel-to-$\boldsymbol{B}$ profiles of the RHS of Eq. (12) for (a) $\rho = 0.02$, (b) 0.1 and (c) 0.2 in $f_{\rm exp} = 1.2$ case; the total (thick solid), the contribution of S (thin solid), d$c_{\rm s}$/ds (thin broken) and dB/ds (thin chain lines).

energy gain from the mirror effect is used directly for this acceleration, which is also seen in Sec. 4.2. In the region of the decelerating supersonic plasma flow (i.e. $s = 13.7 \sim 16.8$ m), the same energy gain is used to heat $T_{\rm i,\parallel}$. Right at the position of the shock wave (i.e. $s \sim 16.8$ m), the same energy gain is lost to electrons via the parallel electric field made by the increase in n. From this example, it can be said that the introduction of the AIP to a plasma fluid model is essential not only for self-consistent treatment of supersonic plasma flows but also for explaining the energy balance in supersonic plasma flow conditions.

5 Conclusion

Advanced divertors are expected to tolerate high heat load predicted in DEMO reactors by obtaining larger plasma wetted areas than a standard divertor by, for example, poloidal/total flux expansion. Supersonic plasma flows become easier to occur in divertors with total flux expansion. It is thus essential to develop a theoretical or numerical model which self-consistently predicts a generation of a supersonic plasma flow. Especially in the widely-used numerical model (i.e. the Braginskii equations), however, an explicit boundary condition of the plasma flow velocity at the sheath entrance in front of divertor plates is necessary in order to solve the parabolic-type equation of parallel plasma momentum.

We have been developing a plasma fluid model incorporating the anisotropic ion pressure (the AIP model). It enables us to describe the equation of parallel plasma momentum as a hyperbolic type keeping the finite effect of the parallel ion viscosity which is solved without an explicit boundary condition on the plasma flow velocity. In this paper, we first compare

plasma profiles from the AIP model with those from the B2 code which is based on the Braginskii equations including cases of decelerating supersonic plasma flows by using pure-poloidal magnetic field systems in order to obtain qualitative insights more simply. Then, we apply the AIP model to a scrape-off layer (SOL)/divertor system, the scale of which is similar to medium-size tokamaks, incorporating super-X divertors (SXDs) with different total flux expansion ratio $f_{\rm exp}$ and investigate characteristics of supersonic plasma flows focusing on effects of $f_{\rm exp}$ and ionization sources in front of divertor plates.

In the study of comparisons between the AIP model and the B2 code, we choose an option for the boundary condition on the plasma flow velocity at the sheath entrance in the B2 code in which the plasma flow velocity is linearly extrapolated if it tends to be higher than the sound speed. Because flux contraction and ionization sources act to decelerate a supersonic plasma flow, we use a flux-contraction system without recycling and a flux-expansion system with finite recycling ratios by using the minimal neutral model in the B2 code. In the former case, the plasma flow velocity in the B2 code is forced to be the sound speed at the sheath entrance due to deceleration in the contracting magnetic field region. It also makes a difference in the magnitude of the plasma density in front of the target plate. In the latter case, we observe a certain range of the recycling ratio with which the plasma flow velocity in the B2 code is forced to be the sound speed at the sheath entrance just like the former flux-contraction case. In this range of the recycling ratio, the effect of the ionization source is large enough to cancel that of flux expansion and hence the supersonic plasma flow decelerates in front of the target. It is, thus, indicated that the option for the boundary condition on the plasma flow velocity we choose does not always give a self-consistent solution as well as fixed boundary conditions which are also usually used [45]. The latter case also demonstrates qualitatively that a self-consistent treatment of supersonic plasma flows is essential for evaluating the atomic and molecular (A&M) processes.

In the application of the AIP model to an SOL/divertor system, a simple neutral model which is similar to the minimal model in the B2 code is also introduced. We examine $f_{\rm exp} = 1.2$ and 1.5 for simulating SXDs as well as $f_{\rm exp} = 0.8$ and 1 for comparison. In $f_{\rm exp} \geq 1$ cases without recycling, supersonic plasma flows are generated in the divertor regions. The profiles of the parallel and perpendicular ion temperatures make it clear that the AIP model can simulate plasmas with highly anisotropic ion temperature which are expected in future fusion devices and that the supersonic plasma flows in SXDs are generated due to a combination of energy gain in the parallel component of ions by the mirror effect and the parallel ambipolar electric field. With finite recycling ratios in SXDs, three patterns of the plasma flows are generated in the divertor region; (i) supersonic plasma flows decelerating in front of the divertor plate, (ii) supersonic plasma flows turning into subsonic with stationary shock waves and (iii) subsonic plasma flows. These patterns can be explained by the Bohm criterion and the balance between ionization sources and flux expansion. Also, the power balance between the parallel, perpendicular components of ions and electrons in the divertor region is comprehensibly explained in the shock-wave case from the viewpoint of the mirror effect, which is thought to be difficult with the Braginskii equations.

In this paper, we apply the Braginskii equations (i.e. the B2 code) only to high-collisionality plasmas. It enables us to exclude the issue of the validity of the approximation introduced to the parallel ion viscosity (i.e. Eq. (8)) because it is derived under an assumption of high collisionality. That is why the upstream plasma profiles in Fig. 2 agree well between the

AIP model and the B2 code. It is demonstrated in Ref. [32], however, that the validity of the approximation for the parallel ion viscosity can be lost in low-collisionality plasmas resulting in qualitative deviations between the AIP model and the B2 code. This is mainly caused by the absolute value symbol introduced in Eq. (10) in order to avoid a generation of unphysical and unstable negative parallel ion viscosity η_{i} in decelerating plasma flows. This absolute value symbol, however, is redundant to approximate the parallel ion viscosity [47] and produces an incorrect approximation in decelerating plasma flows. From this viewpoint, it is considered to be difficult with the Braginskii equations to capture qualitative characteristics of decelerating plasma flows (regardless of whether they are supersonic or subsonic) including stationary shock waves in low-collisionality plasmas like those seen in Fig. 7.

The AIP model presented in this paper is still on a developing stage and has lack of many physical processes which are thought to be important in quantitative numerical simulations such as the radial transport and A&M processes other than the ionization reaction. It is important to consider the effect of the radial particle transport from the divertor region to the private region, which helps generate supersonic plasma flows [60]. Volumetric recombination processes and radiation cooling which become dominant in detached regime can also help generate supersonic plasma flows [34]. It is necessary, therefore, to introduce the AIP model to multi-dimensional plasma fluid codes which are coupled with sophisticated neutral and impurity codes as code packages. As for one-dimensional physics, a generalized modeling of the parallel conductive heat flux in inhomogeneous magnetic fields remains as an issue which can alter temperature profiles even though a flux-limiting procedure is introduced [44]. After developing appropriate models, we are planning to conduct a benchmark study of the AIP model by using experimental data of a tandem mirror device GAMMA 10/PDX [61], which is characterized by a largely diverging magnetic field at the end regions and highly anisotropic ion temperature.

Acknowledgments

Authors are deeply grateful to Dr. K. Shimizu (QST, Japan), Dr. M. Nakamura (QST, Japan), Dr. K. Hoshino (Keio Univ., Japan) and the GAMMA 10/PDX team (PRC, Japan) for fruitful discussion and to Dr. P. Börner (FZJ, Germany) for support on computational matters.

This work is partly supported by the IEA Technology Collaboration Programme on the Development and Research on Plasma Wall Interaction Facilities for Fusion Reactors (PWI TCP) and the NINS program of Promoting Research by Networking among Institutions (Grant Number 01411702).

References

[1] Kukushkin A.S., Pacher H.D., Pacher G.W., Kotov V., Pitts R.A. and Reiter D. 2013 *J. Nucl. Mater.* **438** S203
[2] Kukushkin A.S. and Pacher H.D. 2016 *Nucl. Fusion* **56** 126012
[3] Eich T. *et al* 2013 *Nucl. Fusion* **53** 093031
[4] Hoshino K., Asakura N., Shimizu K., Tokunaga S., Takizuka T., Someya Y., Nakamura M., Utoh H., Sakamoto Y. and Tobita K. 2014 *Plasma Fusion Res.* **9** 3403070

[5] Soukhanovskii V.A. 2017 *Plasma Phys. Control. Fusion* **59** 064005
[6] Ryutov D.D. 2007 *Phys. Plasmas* **14** 064502
[7] Valanju P.M., Kotschenreuther M., Mahajan S.M. and Canik J. 2009 *Phys. Plasmas* **16** 056110
[8] Reimerdes H. *et al* 2017 *Nucl. Fusion* **57** 126007
[9] LaBombard B. *et al* 2015 *Nucl. Fusion* **55** 053020
[10] Hatayama A., Segawa H., Schneider R., Coster D.P., Hayashi N., Sakurai S., Asakura N. and Ogasawara M. 2000 *Nucl. Fusion* **40** 2009
[11] Cohen R.H. and Ryutov D.D. 1999 *Phys. Plasmas* **6** 1995
[12] Cohen R.H. and Ryutov D.D. 2004 *Contrib. Plasma Phys.* **44** 111
[13] Ghendrih Ph. *et al* 2011 *Plasma Phys. Control. Fusion* **53** 054019
[14] Inutake M., Ando A., Hattori K., Tobari H. and Yagai T. 2002 *J. Plasma Fusion Res.* **78** 1352
[15] Inutake M., Ando A., Hattori K., Tobari H., Hosokawa Y., Sato R., Hatanaka M. and Harata K. 2004 *arxiv:physics*/0410205 [physics.plasm-ph]
[16] Petrie T.W. *et al* 2013 *Nucl. Fusion* **53** 113024
[17] Fishpool G. *et al* 2013 *J. Nucl. Mater.* **438** S356
[18] Hayashi Y., Ohno N., Kajita S. and Tanaka H. 2017 *Phys. Plasmas* **24** 062509
[19] Takimoto T., Ishikawa F., Iijima T., Tonegawa A., Sato K. and Kawamura K. 2017 *Fusion Eng. Des.* **124** 235
[20] Stangeby P.C. 2011 Modified 2 Point Model of the SOL to allow for variation in R_{target} http://starfire.utias.utoronto.ca/divimp/publications/2PM-with-R_t-variation-10Aug11-inc.pdf
[21] Schneider R., Bonnin X., Borrass K., Coster D.P., Kastelewicz H., Reiter D., Rozhansky V.A. and Braams B.J. 2006 *Contrib. Plasma Phys.* **46** 3
[22] Kawashima H., Shimizu K., Takizuka T., Sakurai S., Nakano T., Asakura N. and Ozeki T. 2006 *Plasma Fusion Res.* **1** 031
[23] Shimizu K., Takizuka T., Ohya K., Inai K., Nakano T., Takayama A., Kawashima H. and Hoshino K. 2009 *Nucl. Fusion* **49** 065028
[24] Rognlien T.D., Milovich J.L., Rensink M.E. and Porter G.D. 1992 *J. Nucl. Mater.* **196-198** 347
[25] Havlíčková E., Harrison J., Lipschultz B., Fishpool G., Kirk A., Thornton A., Wischmeire M., Elmore S. and Allan S. 2015 *Plasma Phys. Control. Fusion* **57** 115001
[26] Moulton D., Harrison J., Lipschultz B. and Coster D. 2017 *Plasma Phys. Control. Fusion* **59** 065011
[27] Asakura N., Hoshino K., Shimizu K., Shinya K., Utoh H., Tokunaga S., Tobita K. and Ohno N. 2015 *J. Nucl. Mater.* **463** 1238
[28] Umansky M.V., Rensink M.E., Rognlien T.D., LaBombard B., Brunner D., Terry J.L. and Whyte D.G. 2017 *Nucl. Mater. Ene.* **12** 918
[29] Braginskii S.I. 1965 Transport process in a plasma *Reviews of Plasma Physics* vol. **1** ed Leontovich M.A. (New York: Consultants Bureau) p.205
[30] Hoshino K., Shimizu K., Takizuka T., Asakura N. and Nakano T. 2010 *J. Plasma Fusion Res. Ser.* **9** 592
[31] Braams B.J. 1987 NET report no. 68 (EUR-FU/XII-80/87/68)
[32] Togo S., Reiser D., Börner P., Sakamoto M., Ezumi N. and Nakashima Y. 2018 *Plasma Fusion Res.* **13** 3403022
[33] Marchuk O. and Tokar M.Z. 2007 *J. Comput. Phys.* **227** 1597
[34] Marchuk O. and Tokar M.Z. 2008 *Contrib. Plasma Phys.* **48** 164

[35] Isoardi L., Chiavassa G., Ciraolo G., Haldenwang P., Serre E., Ghendrih Ph., Sarazin Y., Schwander F. and Tamain P. 2010 *J. Comput. Phys.* **229** 2220
[36] Goswami R., Artaud J.F., Imbeaux F. and Kaw P. 2014 *Phys. Plasmas* **21** 072510
[37] Takizuka T. and Abe H. 1977 *J. Comput. Phys.* **25** 205
[38] Takizuka T., Tani K., Azumi M. and Shimizu K. 1984 *J. Nucl. Mater.* **128-129** 104
[39] Froese A., Takizuka T. and Yagi M. 2010 *Plasma Fusion Res.* **5** 026
[40] Togo S., Takizuka T., Nakamura M., Hoshino K. and Ogawa Y. 2015 *J. Nucl. Mater.* **463** 502
[41] Togo S., Takizuka T., Nakamura M., Hoshino K., Ibano K., Lang T.L. and Ogawa Y. 2016 *J. Comput. Phys.* **310** 109
[42] Togo S., Takizuka T., Nakamura M., Hoshino K., Ibano K., Lang T.L. and Ogawa Y. 2016 *Contrib. Plasma Phys.* **56** 729
[43] Togo S., Takizuka T., Reiser D., Hoshino K., Ibano K., Li Y., Ogawa Y., Sakamoto M., Ezumi N. and Nakashima Y. 2018 *Contrib. Plasma Phys.* **58** 556
[44] Togo S., Takizuka T., Sakamoto M., Ezumi N., Ogawa Y., Ibano K., Nojiri K., Iijima T., Kinoshita Y., Hara T. and Nakashima Y. 2019 *Plasma Fusion Res.* **14** 2403010
[45] Togo S., Takizuka T., Reiser D., Sakamoto M., Ogawa Y., Ezumi N., Ibano K., Nojiri K., Li Y. and Nakashima Y. 2019 *Nucl. Mater. Energy* **19** 149
[46] Zawaideh E., Najmabadi F. and Conn R.W. 1986 *Phys. Fluids* **29** 463
[47] Fundamenski W. 2005 *Plasma Phys. Control Fusion* **47** R163
[48] Tskhakaya D., Subba F., Bonnin X., Coster D.P., Fundamenski W., Pitts R.A. and JET EFDA Contributors 2008 *Contrib. Plasma Phys.* **48** 89
[49] Reiter D. 1992 The EIRENE code, Version Jan. 92, User manual, KFA Jülich rep., JÜL-2599
[50] Shimizu K., Takizuka T., Sakurai S., Tamai H., Takenaga H., Kubo H. and Miura Y. 2003 *J. Nucl. Mater.* **313-316** 1277
[51] Hyodo I., Hirano M., Miyamoto K., Hoshino K. and Hatayama A. 2003 *J. Nucl. Mater.* **313-316** 1183
[52] Shimizu K. *et al* 1995 *J. Nucl. Mater.* **220-222** 410
[53] Dawson J.M. and Uman M.F. 1965 *Nucl. Fusion* **5** 242
[54] Rognlien T.D. and Brengle T.A. 1981 *Phys. Fluids* **24** 871
[55] Spitzer L. and Härm R. 1953 *Phys. Rev.* **89** 977
[56] Baelmans M. 1993 Dissertation at Katholieke Universiteit Leuven Afd. Toeg. Mechanica, Celestijnenlaan 300 A 3001 Leuven Belgium
[57] Stangeby P.C. 2002 The Plasma Boundary of Magnetic Fusion Devices (Bristol: Institute of Physics Publishing)
[58] Dux R., Peeters A.G., Gude A., Kallenbach A., Neu R. and ASDEX Upgrade Team 1999 *Nucl. Fusion* **39** 1509
[59] Takizuka T. and Hosokawa M. 2000 *Contrib. Plasma Phys.* **40** 471
[60] Takizuka T., Hosowaka M. and Shimizu K. 2001 *J. Nucl. Mater.* **290-293** 753
[61] Nakashima Y. *et al* 2017 *Nucl. Fusion* **57** 116033